

Optical Shaping of Plasma Cavity for Controlled Laser Wakefield Acceleration

Bobbili Sanyasi Rao^{1,2†}, Myung Hoon Cho^{1,3}, Hyung Taek Kim^{1,4#}, Jung Hun Shin¹, Kyung Hwan Oh¹, Jong Ho Jeon¹, Byung Ju Yoo¹, Seong Ha Cho¹, Seong Ku Lee^{1,4}, Chang Hee Nam^{1,5}

¹*Center for Relativistic Laser Science (CoReLS), IBS, Gwangju 61005, Korea*

²*Laser Plasma Division, Raja Ramanna Centre for Advanced Technology, HBNI, Indore 452013, India*

³*Pohang Accelerator Laboratory, Pohang, Gyeongbuk 37673, Korea*

⁴*Advanced Photonics Research Institute, GIST, Gwangju 61005, Korea*

⁵*Department of Physics and Photon Science, GIST, Gwangju 61005, Korea*

[†]*sunnyb@rrcat.gov.in/ #htkim@gist.ac.kr*

Laser wakefield accelerators rely on relativistically moving micron-sized plasma cavities for self-injection, acceleration, and focusing of electrons. Here, we demonstrate transverse shaping of the plasma cavity to produce controlled sub-GeV electron beams, adopting laser pulses with an axially rotatable ellipse-shaped focal spot. We demonstrate the control capability on self-injection, charge and transverse shape of the electron beams produced by rotating the focal spot. We observed that the effect of the elliptical focal spot was imprinted in the profiles of the electron beams and the electron energy increased, as compared to the case of a circular focal spot. We performed 3D PIC simulations which reproduced the experimental results and also revealed dynamics of a new asymmetric self-injection process. This simple scheme offers a novel control method on laser wakefield acceleration to produce tailored electron beams and x-rays for various applications.

The laser wakefield acceleration (LWFA) method has attracted strong attention since its conception [1-3] as a potential alternative to the conventional technology for developing a compact TeV electron-positron collider [4] and ultrashort bright x-ray sources [5]. The LWFA has demonstrated nearly 10 GeV electron beams from 10 cm-scale plasma driven by a petawatt laser pulse in recent experiments [6, 7]. Further, significant efforts were also being made towards the development of practical schemes to efficiently control the injection and acceleration processes to produce controllable high-quality electron beams [8-16] and bright radiation sources [17-21] for a variety of applications.

LWFA exploits strong wakefields (≥ 100 GV/m) in plasma excited by the ponderomotive force (F_p) of an intense laser pulse. The ponderomotive force ($F_p \propto -\nabla I_L$, where I_L is laser intensity) of a transversely focused short-pulse laser displaces plasma electrons in all directions, while heavier ions stay behind. The charge separation results in the formation of a plasma wake wave (also known as plasma “cavity” or “bubble”) when the pulse-length and focal spot radius of the laser match half the plasma wavelength [22, 23]. When the laser pulse attains sufficient intensity for nonlinear wave breaking through self-evolution in the plasma, the electrons from the background plasma can be self-injected into the plasma cavity from its back-end [24]. The injected electrons experience an accelerating force due to the axial component of the wakefield and a transverse focusing force due to the radial component of the wakefield in the plasma cavity. The radial force acts to transversely confine

the accelerating electrons transversely and causes their transverse oscillations, known as “betatron oscillations” around the laser axis, which produces highly directional ultrashort (\sim fs) synchrotron radiation [21].

When a laser pulse is focused perfectly to a perfect circular spot in a plasma, the associated transversely symmetric ponderomotive force produces a transversely symmetric plasma cavity and wakefield. Studies on electron injection in LWFA [25, 26] and emission of betatron radiation [19] mostly consider spherical plasma cavities. In principle, the transverse shape of the plasma cavity can be tailored by shaping the laser focal spot. An optical shaping would enable delicate control on the self-injection and trajectories of electrons in the plasma cavity that can facilitate the control of electron beams and betatron radiation. Earlier, laser pulses with off-centered intensity peak or an asymmetric profile were shown to enable preferential betatron oscillations in a certain plane [27-29] and also enhanced x-ray emission [20]. However, the direct control of the LWFA process and transverse properties of the electron beam by shaping the laser focus has not been shown so far, even though the tuning of LWFA by manipulating the plasma cavity can play a crucial role for controllable electron beams and x-rays.

In this letter, we demonstrated experimentally that the transverse profile of sub-GeV quasi-monoenergetic electron beams and in particular the ellipticity of the electron beam profile could be controlled by using a laser pulse with an ellipse-shaped focal spot. In addition, we showed that the

major axis of the transverse profile and the beam charge of the electron beam could be varied by rotating the focal spot around the laser axis. We demonstrated in experiments and particle-in-simulations that the shaped focal spot could be used for controlling not only the transverse properties of the electron beam but also the self-injection dynamics in LWFA.

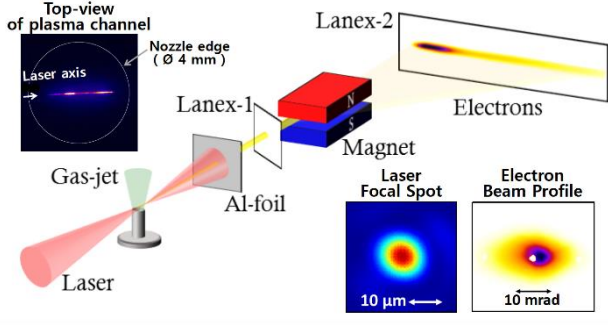


Figure 1. Schematic of the experimental set-up used for laser wakefield acceleration. The images of the laser focal spot and the corresponding electron beam profile without shaping of the laser beam are shown in the inset at bottom-right. The top-view image of the plasma channel is shown in the inset at top-left. The focal spot was nearly circular after correcting with an adaptive optics.

The experiment was performed using a femtosecond Ti:sapphire laser with a peak power of 150 TW. The laser delivered horizontally polarized ultrashort laser pulses of full-width-at-half maximum (FWHM) duration, $\tau_L = 27 \pm 2$ fs. The transverse profile of the laser beam before focusing was circular and had a flat-top intensity distribution with measured FWHM diameter 70 mm. The LWFA experiment was set up inside a vacuum interaction chamber. A schematic of the experimental setup is shown in Fig. 1. The laser beam was focused, using a spherical focussing mirror with f-number 17, into a helium gas jet produced from a cylindrical nozzle with an orifice diameter of 4 mm. The laser focus was kept at a height of 1 mm from the nozzle where the gas jet has 2-mm wide flat-top density profile with 1mm up- and down-ramps along the laser axis. The laser propagation and its interaction length in the helium gas jet plasma were monitored through top-view imaging of the radiation from the plasma.

The electron beams produced by the LWFA was characterized using the diagnostics set up in the laser downstream direction. A thin aluminium foil (Al-foil), kept after the interaction, blocks the residual drive laser beam. The $\text{Gd}_2\text{O}_2\text{S}:\text{Tb}$ scintillating screens (LanexTM) Lanex-1 (kept at a distance of 35cm from the gas jet) and Lanex-2 (kept at a distance of 52cm from the exit of the magnet) imaged with CCD

cameras were used for monitoring electron beam before and after passing through the magnet. The images obtained from the Lanex-1 were used to measure the pointing, transverse shape, divergence, and total charge of the electron beam. A H-type permanent dipole magnet, having 0.96T over 20.5cm length within a pole gap of 8mm, was used for horizontally dispersing the accelerated electron beam to measure its energy spectrum. The Lanex-2 screen was set to detect electrons in the energy range 0.1 - 0.5 GeV for the beam pointed along the drive laser direction. The resolution of electron energy measurement was 2% at 0.1 GeV and 16% at 0.5 GeV by considering the beam divergence of 10 mrad in the dispersion plane.

We have employed an adaptive optics system to correct the wavefront distortion of the laser beam to achieve a good quality focal spot. A typical image of measured focal spot is shown in an inset of the Fig. 1. The focal spot was nearly circular with average w_0 of 17 μm. In order to shape the focal spot, we introduced an ellipse-shaped hard aperture in the laser beam path centred on the beam axis, prior to sending the laser beam onto the focusing mirror. The elliptic aperture has a diameter of 65 mm × 43.3 mm and ellipticity of 1.5. The aperture could be translated in and out of the beam path and could also be rotated about the axis of the laser beam. The introduction of the aperture caused the laser beam to acquire ellipse shape and transmitted nearly 60% of the laser energy.

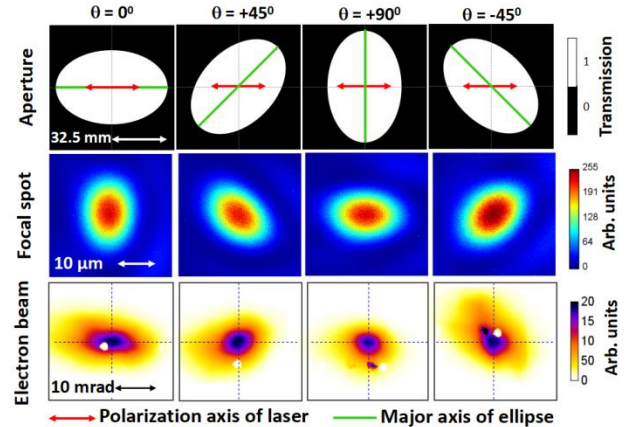


Figure 2. Top row - representative images of the ellipse-shaped hard aperture oriented in four different directions w.r.t. the laser polarization direction, and the corresponding images of the laser focal spot and the electron beam recorded when the aperture was introduced in the drive laser beam. The white dots in the electron beam images are reference markers on Lanex screen used for the calibration of imaging.

The focal spot images of the ellipse-shaped laser beam were measured for different orientations of the ellipse w.r.t. the laser polarization axis, as shown in Fig. 2. The focal spot was clearly elliptical with its

major axis aligned perpendicular to that of the elliptical aperture. The rotation of the focal spot with the rotation of aperture could also be noticed in the figure. The $1/e^2$ radius of the shaped focal spot was measured to be $25\ \mu\text{m} \times 17\ \mu\text{m}$ which gives rise to the ellipticity, $e \approx 1.5$, where we define ellipticity $e = a/b$; a and b are respectively the major and the minor radius of the ellipse. The peak laser intensity, I_L in the focus is $8.4 \times 10^{18}\ \text{W}/\text{cm}^2$ and the corresponding laser strength parameter, $a_0 = 0.85 [I_L (\times 10^{18}\ \text{W}/\text{cm}^2) \lambda^2 (\mu\text{m})]^2 \approx 2$, considering the transmission of the aperture and the energy concentrated in the focal spot. Corresponding to the 60% transmission of the aperture, the laser beam without aperture provided higher peak intensity of $1.7 \times 10^{19}\ \text{W}/\text{cm}^2$ and $a_0 \approx 2.5$.

The LWFA experiment was initially carried out without the elliptic aperture and reproducible electron beams were obtained from self-injected LWFA at plasma density, $n_e \approx 1 \times 10^{19}\ \text{cm}^{-3}$ ($c\tau = 0.8\lambda_p > \lambda_p/2$) from $2.3 \pm 0.1\ \text{mm}$ long plasma channel. The laser power was reduced to about 60% of maximum power in order to match the laser energy on target with and without aperture. The electron beam measurements were performed for several laser shots and determined the mean and standard error of relevant beam parameters. Images of the typical electron beam profile and the laser-plasma channel are shown in the insets of Figure 1. In spite of the circular focal spot, the electron beam profile displays ellipticity in its angular divergence elongated along the laser polarization axis, indicating the overlap of accelerating electrons with the drive laser field inside the back-half of the bubble [29]. The direct influence of the laser field was further evident during the experiment from the observation of larger ellipticity at higher plasma density and/or laser power. The FWHM contour of the electron beam profile was fitted to a closest ellipse to quantify the various parameters associated with the ellipse-shaped electron beam. The electron beam has divergence angles $10.2 \pm 0.7\ \text{mrad}$ and $6.0 \pm 0.4\ \text{mrad}$ along the horizontal and the vertical planes respectively. The ellipticity of the electron beam was 1.74 ± 0.10 and the orientation of its major axis was $-5.2^\circ \pm 3.8^\circ$. The root-mean-square (rms) pointing of the electron beams was $1.9\ \text{mrad}$ and $1.7\ \text{mrad}$ in both the planes.

To demonstrate the effect of ellipse-shaped focal spot on LWFA, the elliptical aperture was inserted in the laser beam. The images in the third row of Figure 2 show the typical profiles of electron beams recorded for different orientations of the focal spot w.r.t. the laser polarization axis. Figure 2 clearly indicates that the major axis of the electron beam follows the rotation angle of the aperture except for the case of

$\theta=90^\circ$. In the case of $\theta=90^\circ$, the major axis of the elliptic electron beam possibly could not be aligned with that of the aperture due to the dominant effect of the laser polarization along the horizontal axis. The energy spectra of the electron beams were compared for the two cases obtained with and without the aperture in the laser beam path for the same laser energy on target. We found that the shaped laser focus can stabilize the electron injection resulting in electron beams with better reproducibility. The averaged energy spectra with rms errors measured with and without the aperture are shown in Fig. 3. The electron beams with the elliptic focal spot had enhanced stability and higher peak energy compared to the circular focus result. We could not observe considerable change in the peak energy of the electron beam with the rotation of the focal spot.

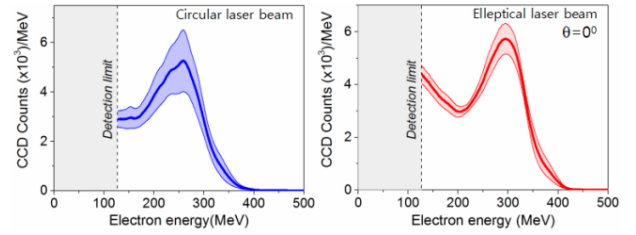


Figure 3. Experimentally measured energy spectra of electron beams produced from LWFA with circular and elliptical focus.

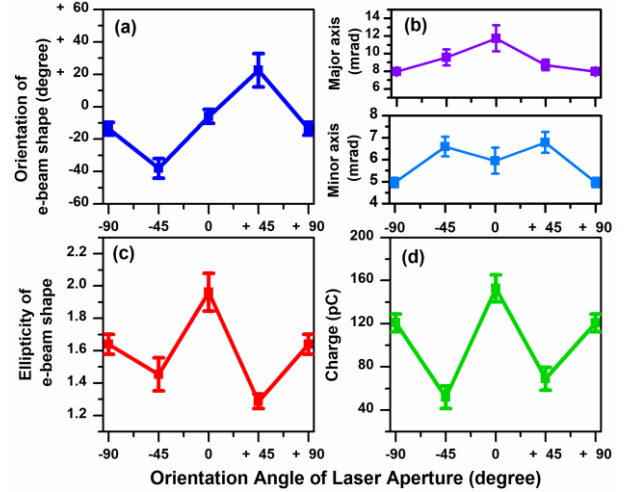


Figure 4. Variation of electron beam parameters with change in orientation of the ellipse shaped laser beam w.r.t. its polarization. For comparison, the electron beam parameters with circular laser beam are (a) orientation: -5.2 ± 3.8 , (b) horizontal divergence: $-10.2 \pm 0.73\ \text{mrad}$ and vertical divergence: $6.0 \pm 0.44\ \text{mrad}$, (c) ellipticity: 1.7 ± 0.10 , and (d) charge: $120 \pm 10\ \text{pC}$.

The effect of the shaped focal spot on the spatial parameters and the charge of the electron beam is shown in details in Fig. 4. As discussed earlier, the major axis of an electron beam obviously rotated with the rotation of the aperture except for the orientation of 90° . However, the effect of asymmetric wakefield

on the transverse profile of the electron beam can be identified from Fig. 4b. The angular divergence along the major axis is highest for the 0° orientation of the aperture and the lowest for 90° , which highlights the asymmetry (higher strength along the minor axis of the focus) of transverse forces. The variation of different spatial properties of the electron beam shown in Fig. 4 can originate from the combined effect of the drive laser field and the asymmetry in the transverse wakefield caused by the elliptical focal spot. These results clarify the crucial role of transverse forces of the wakefield in controlling LWFA and electron trajectories. More interestingly, the charge of the accelerated electron beam shows a strong dependence on the orientation of the elliptical focal spot w.r.t. the polarization axis. This indicates the delicate influence of the transverse asymmetry of wakefield on electron injection dynamics. It should be noted that the highest charge is injected when the major axis of the elliptical spot is perpendicular to the laser polarization axis and the least charge ($\approx 25\%$ of maximum charge) is injected for $\pm 45^\circ$. The difference in the charge for 0° and 90° is also noticeable, although the difference of about 25 % is less drastic compared to the cases of $\pm 45^\circ$.

We performed 3D PIC simulation using the code JoPIC [31] for plasma density of $4.5 \times 10^{19} \text{ cm}^{-3}$ and for the horizontally polarized laser pulses with duration, $c\tau = 25\text{fs}$ ($\approx \lambda_p/2$) and circular (elliptical) focal spot size $20\mu\text{m}$ ($30\mu\text{m} \times 20\mu\text{m}$) at FWHM. The energy content for both cases is kept constant, i.e. $a_0 = 2.7$ for the circular focus and 2.2 for the elliptical focus. The plasma density profile is chosen close to the experimental conditions and the laser focal position is 3 mm where it is behind the plasma target. Simulations clearly show an electron beam with elliptic profile (Fig. 5a) and higher energy (Fig. 5b), even though the initial a_0 of the elliptical laser focus is lower than the circular focal spot, as observed in the experiment. Figure 5c compares the plasma cavity structures at the moments of electron injection. The formation of an elliptical plasma cavity is clearly shown for the elliptic focal spot. Electrons are injected with axial symmetry in the circular case, while electrons are injected asymmetrically in the elliptic case (more electrons vertically injected following the major axis of the laser focus). Even though the injection is vertically asymmetric, as shown in Fig. 5 (a), the divergence of the electron beam was horizontally elliptic due to the strong wakefield along the horizontal axis (x -axis). It is observed in the simulation that the higher energy beam produced due to early injection (dashed line) for elliptical focus, as shown in Fig.5 (d). Both the cases

indicate that the injection occurs at about $a_0 = 3.0$. Even though the elliptical laser focus has lower initial a_0 , the broader beam diameter along the major axis of the aperture produces stronger a_0 earlier and drives stronger wakefield than that of the circular laser focus.

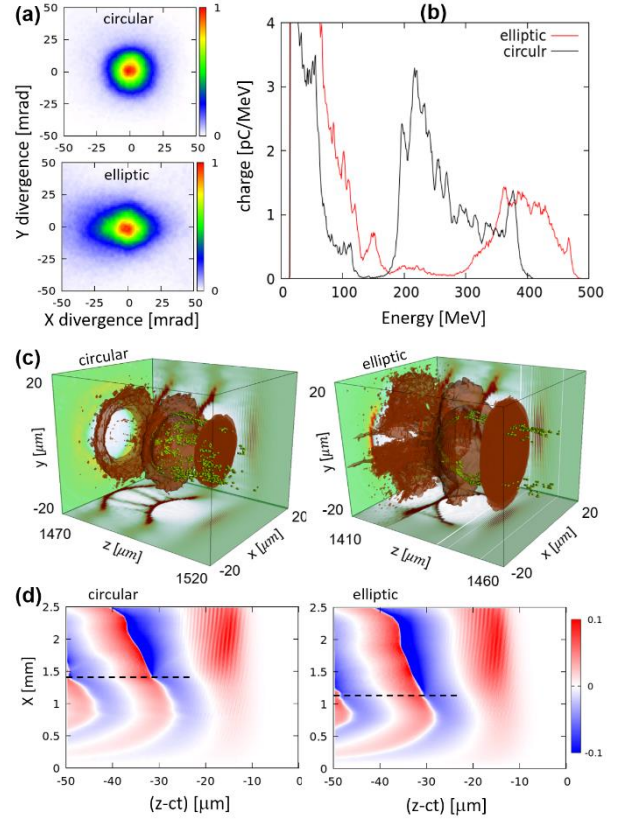


Figure 5. 3D PIC simulation results of LWFA with circular and elliptical focal spots containing the same laser energy: (a) spatial profiles, (b) energy spectra of the electron beams, (c) electron injection in the plasma cavity, and (d) evolution of the wakefield (injection point shown with a dashed horizontal line).

In previous studies, LWFA with asymmetric plasma cavity has been studied with a tilted wavefront [28] or astigmatic aberration [30] of a driving laser pulse to control electron beam direction or to study the angular-momentum evolution of electron beams, respectively. In addition, the generation of an elliptic electron beam along the laser polarization axis, as we observed with circular laser spot, was studied to originate from the direct laser interaction of an accelerated electron beam in the first cavity [29]. In this study, we proved for the first time that the elliptically-shaped laser beams without aberrations or wavefront tilts can be an intrinsic and direct method to control the plasma cavity structure that results in the imprinting of laser profile on the electron beam. The apparent correlation between laser focal spot and electron beam could be verified owing to the aberration-free laser beam obtained with the adaptive

control of laser wavefront. We could also decouple the effect of asymmetric plasma cavity and laser polarization by observing the electron beam shape rotating the elliptic focal shape. Our investigations clearly demonstrated that not only the transverse trajectories of the electrons in the bubble (and consequent modification of the electron beam shape) but also the injection dynamics could be delicately tuned by the choice of the elliptical focal spot and its orientation w.r.t. the laser polarization. This simple technique can facilitate also the control of the betatron motions of electrons in plasma cavity for generating x-rays with tunable polarization [32].

In conclusion, we demonstrated that the transverse shaping of a laser focal spot improved the stability and energy of electron beams produced by effectively controlling the transverse shape of plasma cavities in LWFA. The cavity shaping and its rotation provided the control on electron injection dynamics and the consequent variation of accelerated electron charge, energy, and the plane of betatron oscillations. The ability to control the electron trajectories through the scheme can be exploited further in future for producing tunable high energy electron and polarized synchrotron x-ray beams efficiently from LWFA. The method of transverse shaping of wakefields can also be employed immediately after LWFA for an external control of electron beams with the desired shape at a target location. With adaptive optics available at high power laser facilities, in situ focal spot shaping can be routinely done in a feedback loop to accomplish electron beams and x-rays with desired characteristics.

The authors would like to acknowledge the supports by the Institute for Basic Science (IBS-R012-D1) and by the Research on Advanced Optical Science and Technology grant funded by GIST.

- [1] T. Tajima and J. M. Dawson, *Phys. Rev. Lett.* **43**, 267 (1979).
- [2] E. Esarey, C. B. Schroeder, and W. P. Leemans, *Rev. Mod. Phys.* **81**, 1229 (2009).
- [3] C. Joshi, *IEEE Trans. Plasma Sci.* **49**, 3134 (2017).
- [4] C. B. Schroeder, E. Esarey, C. G. R. Geddes, C. Benedetti and W. P. Leemans, *Phys. Rev. Special Topics* **13**, 101301 (2010).
- [5] M. E. Couprie, A. Loulergue, M. Labat, R. Lehe and V. Malka, *J. Phys. B: At. Mol. Opt. Phys.* **47**, 234001 (2014).
- [6] H. T. Kim, J. H. Shin, C. Aniculaesei, B. S. Rao, V. B. Pathak, M. H. Cho, C. Hojbota, S. K. Lee, J. H. Sung, H. W. Lee, J. W. Yoon, K. Nakajima and C. H. Nam, *The 46th European Physical Society Conference on Plasma Physics*, p. **11.204** (2019).
- [7] A. J. Gonsalve et al., *Phys. Rev. Lett.* **122**, 084801 (2019).
- [8] M. H. Cho, V. B. Pathak, H. T. Kim, and C. H. Nam, *Scientific reports* **8**, 16924 (2018).
- [9] J. Faure, C. Rechatin, A. Norlin, A. Lifschitz, Y. Glinec, and V. Malka, *Nature (London)* **444**, 737 (2006).
- [10] A. Pak, K. A. Marsh, S. F. Martins, W. Lu, W. B. Mori, and C. Joshi, *Phys. Rev. Lett.* **104**, 025003 (2010).
- [11] B. B. Pollock et al., *Phys. Rev. Lett.* **107**, 045001 (2011).
- [12] A. J. Gonsalves et al., *Nat. Phys.* **7**, 862 (2011).
- [13] B. S. Rao et al., *Appl. Phys. Lett. Appl. Phys. Lett.* **102**, 231108 (2013).
- [14] A. Buck et al., *Phys. Rev. Lett.* **110**, 185006 (2013).
- [15] R. Lehe et al., *Phys. Rev. Lett.* **111**, 085005 (2013).
- [16] B. S. Rao et al., *Phys. Rev. ST Accel. Beams* **17**, 011301 (2014).
- [17] J. Wenz et al., *Nat. Photonics* **13**, 263 (2019).
- [18] J. Luo, M. Chen, M. Zeng, J. Vieira, L. L. Yu, S. M. Weng, L. O. Silva, D. A. Jaroszynski, Z. M. Sheng and J. Zhang, *Sci. Rep.* **6**, 29101 (2016).
- [19] S. Corde, K. Ta Phuoc, R. Fitour, J. Faure, A. Tafzi, J. P. Goddet, V. Malka, and A. Rousse, *Phys. Rev. Lett.* **107**, 255003 (2011).
- [20] S. P. D. Mangles et al., *Appl. Phys. Lett.* **95**, 181106 (2009).
- [21] S. Corde, K. Ta Phuoc, G. Lambert, R. Fitour, V. Malka, A. Rousse, A. Beck and E. Lefebvre, *Rev. Mod. Phys.* **85**, 1 (2013).
- [22] A. Pukhov and J. Meyer-ter-Vehn, *Appl. Phys. B Lasers Opt.* **74**, 355–361 (2002).
- [23] W. Lu, C. Huang, M. Zhou, W. B. Mori, and T. Katsouleas, *Phys. Rev. Lett.* **96**, 165002 (2006).
- [24] W. Lu, M. Tzoufras, C. Joshi, F. S. Tsung, W. B. Mori, J. Vieira, R. A. Fonseca, and L. O. Silva, *Phys. Rev. ST Accel. Beams* **10**, 061301 (2007).
- [25] I. Kostyukov, E. Nerush, A. Pukhov, and V. Seredov, *Phys. Rev. Lett.* **103**, 175003 (2009).
- [26] S. Kalmykov, S. A. Yi, V. Khudik, and G. Shvets, *Phys. Rev. Lett.* **103**, 135004 (2009).
- [27] Y. Glinec, J. Faure, A. Lifschitz, J. M. Vieira, R. A. Fonseca, L. O. Silva, and V. Malka, *Europhys. Lett.* **81**, 64001 (2008).
- [28] A. Popp et al., *Phys. Rev. Lett.* **105**, 215001 (2010).
- [29] C. Thauray, E. Guillaume, S. Corde, R. Lehe, M. Le Bouteiller, K. Ta Phuoc, X. Davoine, J. M. Rax, A. Rousse, and V. Malka, *Phys. Rev. Lett.* **111**, 135002 (2013).
- [30] S. P. D. Mangles et al., *Phys. Rev. Lett.* **96**, 215001 (2006).
- [31] M. H. Cho et al., *New J. Phys.* **17**, 043045 (2015)
- [32] Andreas Döpp et al., *Light: Science & Applications* **6**, e17086 (2017).